Available online at www.sciencedirect.com
ScienceDirect
Journal of Solid State Chemistry 180 (2007) 974–980
JOURNAL OF SOLID STATE CHEMISTRY
www.elsevier.com/locate/jssc

Ab initio structural, electronic and optical properties of orthorhombic $CaGeO_3$

J.M. Henriques[a], E.W.S. Caetano[b,*], V.N. Freire[c], J.A.P. da Costa[c], E.L. Albuquerque[a]

[a]*Departamento de Física Teórica e Experimental, Universidade Federal do Rio Grande do Norte, 59072-900 Natal, Rio Grande do Norte, Brazil*
[b]*Centro Federal de Educação Tecnológica do Ceará, Avenida 13 de Maio, 2081, Benfica, 60040-531 Fortaleza, Ceará, Brazil*
[c]*Departamento de Física, Universidade Federal do Ceará, Centro de Ciências, Caixa Postal 6030, Campus do Pici, 60455-760 Fortaleza, Ceará, Brazil*

Received 23 September 2006; received in revised form 13 December 2006; accepted 26 December 2006
Available online 10 January 2007

Abstract

Orthorhombic $CaGeO_3$ is studied using density-functional theory (DFT) considering both the local density and generalized gradient approximations, LDA and GGA, respectively. The electronic band structure, density of states, dielectric function and optical absorption are calculated. Two very close indirect ($S \rightarrow \Gamma$) and direct ($\Gamma \rightarrow \Gamma$) band gap energies of 1.68 eV (2.31 eV) and 1.75 eV (2.41 eV) were obtained within the GGA (LDA) approximation, as well as the effective masses for electrons and holes. Comparing with orthorhombic $CaCO_3$ (aragonite), the substitution of carbon by germanium changes the localization of the valence band maximum of the indirect transition, and decreases by almost 2.0 eV the Kohn–Sham band gap energies.

PACS: 61.43.Bn; 71.15.Mb; 72.80.Sk; 78.20.Ci

Keywords: Orthorhombic $CaGeO_3$; Structural properties; Band structure; Effective masses; Optical absorption; Dielectric function

1. Introduction

Calcium germanate ($CaGeO_3$) belongs to the pyroxenoid group, with each germanium (coordination number IV) atom connected to six oxygen atoms, forming a tridimensional array of GeO_6 tilted octahedra (see Fig. 1). The calcium atoms are inserted between them, resembling the structure of $CaSiO_3$ in the perovskite phase. Under normal conditions of pressure and temperature, $CaSiO_3$ assumes a triclinic structure, with the unit cell containing two chains of tilted SiO_4 tetrahedral groups along the *b*-axis. At ambient conditions, $CaGeO_3$ crystals are orthorhombic (*Pbnm* symmetry), while under pressure it changes first to a rhodonite-like structure at 6 GPa, which is further transformed into a perovskite-form at about 15 GPa [1]. Since $CaGeO_3$ can be quenched to ambient condition, together with $CaSiO_3$, $MgSiO_3$ and others ABO_3 structures, it has being mainly studied for the understanding of the mechanisms that lead to the stabilization of the various perovskite structures, a long standing problem in material science [2].

The major calcium germanate analogs are the silicate $CaSiO_3$ and the carbonate $CaCO_3$. The former has geophysical importance as one of the main materials considered in modelling the dynamics and evolution of the Earth's lower mantle; the latter is one of the most abundant minerals in the Earth surface, with industrial (plastic, rubbers, papers, paints, etc.) and implant applications. There are many theoretical *ab initio* studies on $CaSiO_3$ in the perovskite phase [2–7], but only one on $CaSiO_3$ triclinic [8]. In this case, the band structure, density of states, Kohn–Sham band gap, effective masses, and optical absorption were obtained by first-principles quantum mechanical calculations after optimization of the unit cell parameters and atomic coordinates. On the other hand,

*Corresponding author. Departamento de Física, Universidade Federal do Ceará, Centro de Ciências, Caixa Postal 6030, Campus do Pici, 60455-760 Fortaleza, Ceará, Brazil. Fax: +55 85 4008 9450.
E-mail address: ewcaetano@gmail.com (E.W.S. Caetano).

0022-4596/$ - see front matter © 2007 Elsevier Inc. All rights reserved.
doi:10.1016/j.jssc.2006.12.029

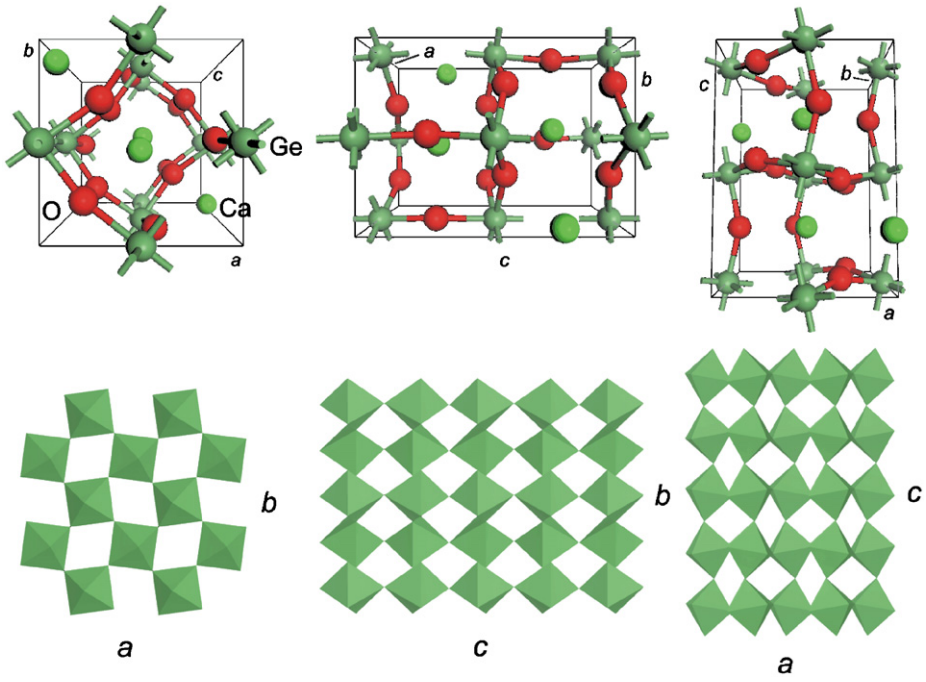

Fig. 1. Crystal structure of orthorhombic $CaGeO_3$. Each germanium (IV) atom is connected to six oxygen atoms, forming a tridimensional array of GeO_6 tilted octahedra with calcium atoms inserted between them. Top: different views of the unit cell and atomic nomenclature. Bottom: tilted GeO_6 octahedra build up the orthorhombic phase.

calcium carbonate ($CaCO_3$) has three polymorphs: calcite (rhombohedral), aragonite (orthorhombic), and vaterite (orthorhombic). A theoretical study on the structure and bonding of calcite was performed by Skinner et al. [9]. They have obtained an indirect energy gap $E_{G(D\to Z)} = 4.4 \pm 0.35$ eV for calcite, which is well below the experimental value of 6.0 ± 0.35 eV [10]. Recently, Medeiros et al. [11] have investigated, by quantum mechanical first-principles calculations, the structural, electronic, and optical properties of $CaCO_3$ aragonite (orthorhombic). The band gap energy was predicted to be ~1 eV smaller than that of calcite (rhombohedral), and two absorption regimes were shown to exist: the first one with weak absorption in the 4.4–6.3 eV range associated to transitions involving mainly *p*-like states of dominating oxygen character; the other with stronger absorption, ruled by $p \to d$ transitions.

For the best of our knowledge, there is no scientific report so far on *ab initio* calculations of orthorhombic $CaGeO_3$ properties. The focus of this work is to simulate structural and optoelectronic properties of calcium germanate by applying quantum chemical first-principles calculations using the density functional theory (DFT) within the local density and generalized gradient approximations framework, LDA and GGA, respectively. A comparison of the results with those of $CaSiO_3$ triclinic and $CaCO_3$ aragonite is performed, revealing the effect of the C, Si → Ge replacement on the electronic structure by looking to the changing pattern of the atomic contributions to the density of states in the simulated crystals, and to the energy band structure as well as optical properties.

2. Calculation methodology

Quantum mechanical first-principles calculations for orthorhombic $CaGeO_3$ were performed using the CASTEP code [12] within the DFT formalism [13,14]. To improve over the total local-density approximation (LDA) [14,15] to the exchange-correlation (XC) energy [16], the generalized gradient approximation (GGA) was also considered [17,18]. For geometry optimization, ultrasoft Vanderbilt-type pseudopotentials [19] were used considering the following electronic configurations: Ca-$3s^2 3p^6 4s^2$, Ge-$4s^2 4p^2$, and O-$2s^2 2p^4$. Ultrasoft pseudopotentials help to reduce the computational cost of first-principles electronic structure calculations by decreasing the energy cutoff of the plane-wave basis set. The XC functional for the LDA calculation is standard [20,21], while for the GGA the Perdew–Burke–Ernzerhof (PBE) functional [22] was chosen. Results for bulk materials obtained with the PBE functional are, in general, very similar to the commonly used PW91 functional [23]. A Monkhorst–Pack $6 \times 6 \times 4$ sampling was used to evaluate integrals in the reciprocal space [24]. This Monkhorst–Pack grid is enough to give a well-converged electronic structure due to the flatness of the $CaGeO_3$ valence bands.

The lattice parameters and the atomic positions were optimized by seeking a total energy minimum for the $CaGeO_3$ unit cell, which is depicted in Fig. 1. The unit cell dimensions and internal atomic coordinates of orthorhombic $CaGeO_3$ measured by X-ray diffraction [25] were used as input. In order to perform the geometry optimization,

the following convergence thresholds were considered for two successive self-consistent steps: (i) total energy change smaller than 0.5×10^{-5} eV/atom; (ii) maximum force over each atom below 0.01 eV/Å; (iii) pressure smaller than 0.02 GPa; (iv) maximum atomic displacement not exceeding 0.5×10^{-3} Å. The Pfrommer et al. minimizer [26] was employed to carry out the unit cell optimization. For each self-consistent field step, the electronic minimization parameters were: (i) total energy/atom convergence tolerance of 0.5×10^{-6} eV ; (ii) eigenenergy threshold of 0.1190×10^{-6} eV at most; (iii) a convergence window of three cycles.

The basis set cutoff energy for our calculations was 500 eV and its quality was kept fixed while taking into account changes of the unit cell volume throughout the search for the optimal geometry. In order to secure the accuracy of our results, we performed geometry optimizations using a larger energy cutoff of 600 eV. The comparison of both outputs revealed that an increase of 100 eV in the quality of the basis set decreases the unit cell total energy by only 0.004% at most, and the first three decimal digits of the lattice parameters do not change at all in both LDA and GGA computations.

After obtaining the unit cell and atomic positions, the electronic band structure and the density of states (total and partial, and the relative contribution of each atom) were evaluated, as well as the dielectric function and optical absorption. We have used the same XC functionals of the energy minimization, although replacing the ultrasoft pseudopotentials by norm-conserved ones [27] with an energy cutoff of 700 eV. Such replacement is necessary due to limitations of the CASTEP code to include some contributions to the optical properties related to the use of ultrasoft pseudopotentials. Increasing the energy cutoff of the basis set to 800 eV changed the electronic eigenenergies by 1 meV at most. Effective masses at the extrema of the valence and conduction bands were estimated by quadratic interpolation of the corresponding band curves following the scheme of Henriques et al. [8]. The complex dielectric function and the optical absorption $\alpha(\omega)$ of orthorhombic $CaGeO_3$ were calculated following the same scheme of previous works [8,11]. This scheme works as follows: first, optical absorption was obtained from the imaginary part of the complex dielectric function, given by

$$\varepsilon_2(\omega) = \frac{2e^2\pi}{\Omega\varepsilon_0} \sum_{\mathbf{k},v,c} |\langle\psi_{\mathbf{k}}^c|\hat{\mathbf{u}}\cdot\mathbf{r}|\psi_{\mathbf{k}}^v\rangle|^2 \delta(E_{\mathbf{k}}^c - E_{\mathbf{k}}^v - \hbar\omega), \quad (1)$$

where ω is the light frequency, $\psi_{\mathbf{k}}^c$ and $\psi_{\mathbf{k}}^v$ are, respectively, the conduction and valence band wavefunctions at $\mathbf{k}$ calculated within the DFT approach. The vector points along the polarization of the incident electric field. The real part ε_1 of the dielectric function is obtained from the imaginary part ε_2 using the Kramers–Kronig relationship [28,29]. The imaginary and real parts of the refraction index (k and n, respectively) are related to ε_1 and ε_2 through:

$$\varepsilon_1 = n^2 - k^2\varepsilon_2 = 2nk. \quad (2)$$

Finally, the optical absorption is given by

$$I(\omega) = \frac{2k\omega}{c}. \quad (3)$$

Although other physical parameters (reflection coefficient, loss function and optical conductivity) were obtained by using our numerical approaches, they are not presented here.

3. Results and discussions

3.1. Volume and geometry optimization

The structural parameters of orthorhombic $CaGeO_3$ calculated after geometry optimization through the DFT-LDA and the DFT-GGA approximations are shown in Table 1, together with the experimental data of Sasaki et al. [25]. In both cases, a good agreement with the experimental data is observed. The lattice parameters calculated within GGA are consistently bigger than those found through LDA calculation and the experimental data. They are coherent with the results found by comparison to other compounds [17,18] and the well-known underbinding effect for this kind of functional. The GGA overestimates the actual orthorhombic $CaGeO_3$ lattice parameters a, b, and c by 1.14%, 2.01%, and 1.34%, respectively. The GGA-calculated unit cell volume is 4.56% bigger than the experimental one, while the LDA-calculated is 5.23% smaller, since LDA overestimates the strength of interatomic interactions. After convergence using the GGA functional, the final average pressure was −0.0076 GPa, and the symmetrized stress tensor components were $\varepsilon_{xx} = 0.002046$ GPa, $\varepsilon_{yy} = 0.010546$ GPa, and $\varepsilon_{zz} = 0.010233$ GPa. The stress is hydrostatic.

A comparison of the bond lengths and angles between our theoretical results for orthorhombic $CaGeO_3$ and orthorhombic $CaSiO_3$, the latter with lattice parameters $a = 5.0517$ Å, $b = 5.0517$ Å, $c = 7.1442$ Å, and space group *Pbnm* [30], is shown in Table 2. We did not present a comparison with orthorhombic $CaCO_3$ (vaterite) due to the different connectivity exhibited by carbon and oxygen atoms (in this CO_3 compound, planar groups, not

Table 1
Comparison between experimental [25] and calculated structural parameters for the $CaGeO_3$ orthorhombic unit cell

	Exp. (Å)	LDA (Å)	LDA-Exp. (%)	GGA (Å)	GGA-Exp. (%)
a	5.2607	5.1624	−1.87	5.3205	+1.14
b	5.2688	5.1832	−1.62	5.3749	+2.01
c	7.4452	7.3086	−1.83	7.5452	+1.34
	Exp. (Å^3)	LDA (Å^3)		GGA (Å^3)	
V	206.36	195.56	−5.23	215.77	+4.56

Table 2
Comparison between experimental [25] and calculated interatomic distances and angles for the $CaGeO_3$ orthorhombic crystal

	Smallest interatomic distance (Å)				Angle (degree)				
	Ge–O	Ge–Ca	O–Ca	Ca–Ca	Ge–O–Ge		O–Ge–O		
					z	*xy*	α	β	γ
LDA	1.897	3.021	2.284	3.607	158.222	157.372	90.006	90.277	90.833
GGA	1.941	3.101	2.331	3.710	155.336	154.744	90.417	90.622	90.752
Exp	1.897	3.105	2.346	3.685	160.354	158.940	90.263	90.269	90.792
	Si–O	Si–Ca	O–Ca	Ca–Ca	Si–O–Si		O–Si–O		
$CaSiO_3$	1.786	3.094	2.526	3.572	180	180	90	90	90

Data of orthorhombic $CaSiO_3$ is also shown [30]. Ge–O–Ge angles are taken for bonds along *z*-axis and parallel to the *xy* plane, while O–Ge–O angles are presented in crescent order (α, β and γ). The remaining O–Ge–O angles belonging to the GeO_6 octahedra are obtaining by subtracting these values from 180°.

octahedra, are formed). We see that, as expected, calculated Ge–O bond lengths are smaller and larger than X-ray measurements, for LDA and GGA approximations, respectively. In comparison to $CaSiO_3$, the Ge–O bond is larger than the Si–O bond by 0.1 Å approximately. The shortest distance between Ge and Ca atoms is also presented, and is smaller than the experimental value (3.105 Å) for both LDA (3.021 Å) and GGA (3.101 Å) calculations, the GGA value being very close to the experimental data (only 0.004 Å smaller). The O–Ca closest neighbors are separated by 2.284 Å (LDA), 2.331 Å (GGA), and 2.346 Å (experimental). On the other hand, Ca–Ca closest neighbors are 3.685 Å apart from experimental data, but are closer within the LDA (3.607 Å) approximation, and farther within the GGA (3.710 Å) one. Ge–O–Ge angles are considered along the *z*-axis and within the *xy* plane. The LDA values are smaller than but closer to experimental data in comparison with GGA values. O–Ge–O angles within GeO_6 are also presented in crescent order, $\alpha<\beta<\gamma$. LDA values are larger than experimental ones for both β and γ, but smaller for α. For the GGA angles, comparing with the X-ray measurements we have smaller γ (by only −0.04%), while α and β are larger. In perovskite $CaSiO_3$ all O–Si–O (Si–O–Si) angles are 90° (180°) as expected due to the absence of tilting in SiO_6 octahedra.

3.2. Band structure, density of states and effective masses

Fig. 2 shows the band structure near the main Kohn–Sham band gap of $CaGeO_3$ according to the GGA (solid) and LDA (dotted) calculations. LDA eigenenergies are larger for the conduction bands and smaller for the valence bands, resulting in larger LDA band gaps in comparison to GGA. This difference is almost constant, practically the same amount of 1 eV if we consider the direct gaps at the *S*, *X*, *Y*, and $U \rightarrow T$ valence band extrema. At the Γ point, however, this discrepancy decreases to 0.6 eV, indicating that a rigid shift of the LDA eigenenergies is not good enough to fairly reproduce the GGA results.

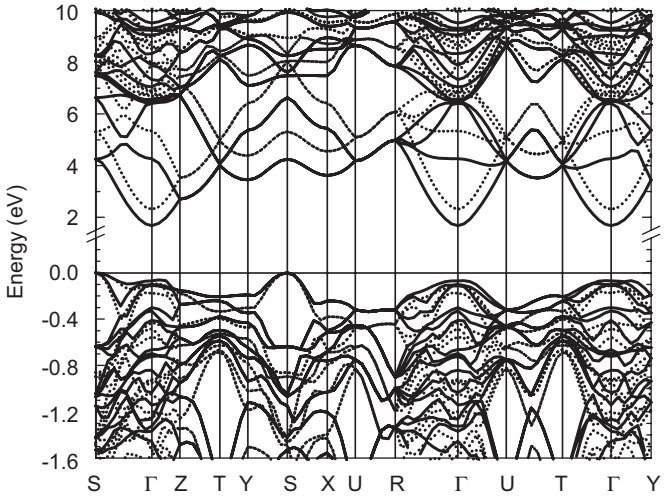

Fig. 2. Orthorhombic $CaGeO_3$ band structure calculated using LDA (dotted) and GGA (solid) functionals. The top valence bands have been aligned at the Γ point (zero energy).

Considering the full GGA band structure (not shown here), there are four energy bands close to −38 eV, originating from Ca-3*s* levels (see Fig. 3), 12 bands near −20 eV with strong contribution from Ca-3*p* states, and 12 bands between −19 and −15 eV which are mainly O-2*s* in character. The uppermost valence bands count is 36, resulting mostly from O-2*p* orbital. Twenty conduction bands were calculated, mixing contributions from calcium, oxygen, Ge-4*s* and Ge-4*p* states, as indicated in Fig. 3. Comparing the density of states predicted for $CaGeO_3$ with the calculated for $CaSiO_3$ [8], we note the absence of Ca-3*d* contributions to the lowermost conduction bands. It seems that the replacement of Si by Ge in some way prevents the formation of Ca 3*d*-related excited electronic levels, at least for the first 20 conduction bands of orthorhombic $CaGeO_3$. This result, however, must be considered with some care, because it is well known that simple GGA calculations tend to poorly describe empty states and *d* states (both filled and empty).

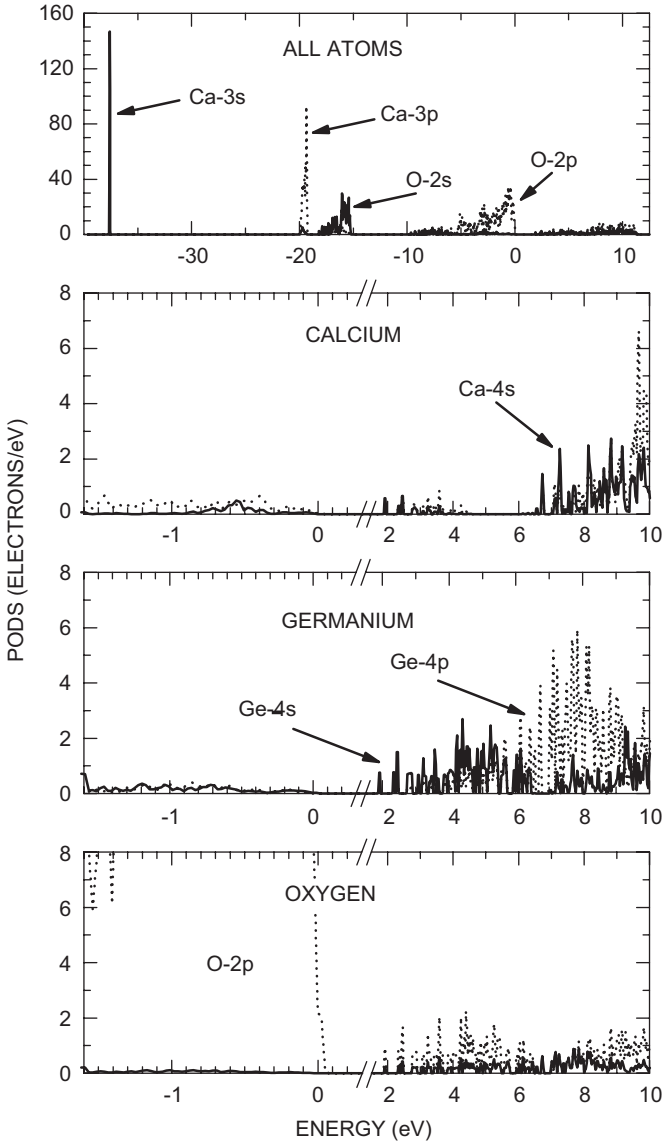

Fig. 3. Partial density of states for electrons in orthorhombic $CaGeO_3$ including contributions from all atoms and contributions from each atom according to the angular momentum. Solid lines: *s* contribution; dotted lines: *p* contribution.

The smallest Kohn–Sham band gap calculated is indirect, between the valence band maximum at $S(-0.5, 0.5, 0)$ and the conduction band minimum at $\Gamma(0,0,0)$. For the LDA calculation, the $S \rightarrow \Gamma$ energy gap is 2.31 eV, while for the GGA we obtain 1.68 eV. We note that due to the approximate nature of DFT functionals, the theoretically calculated energy gaps are inaccurate and somewhat smaller than the experimental measurements. Therefore, the smallest actual band gap of $CaGeO_3$ must be larger than 2.31 eV. The $\Gamma \rightarrow \Gamma$ direct transition involves an energy change of 2.41 eV in the LDA, and 1.75 eV in the GGA. In contrast, according to the LDA calculations of Henriques et al. [8], $CaSiO_3$ presents a wide indirect Kohn–Sham band gap of 5.43 eV between the Q and Γ points, and a direct band gap of 5.52 eV for $\Gamma \rightarrow \Gamma$ transitions.

Table 3
Carriers effective masses of $CaGeO_3$ orthorhombic along some symmetry directions

Valence band	LDA	GGA	Conduction band	LDA	GGA
$m_{lh}(S \rightarrow \Gamma)$	1.00	1.23	$m_e(\Gamma \rightarrow S)$	0.41	0.46
$m_{hh}(S \rightarrow \Gamma)$	4.19	4.26	$m_e(\Gamma \rightarrow Z)$	0.35	0.39
$m_h(S \rightarrow Y)$	1.89	2.39	$m_e(\Gamma \rightarrow R)$	0.42	0.47
$m_h(S \rightarrow X)$	1.25	1.43	$m_e(\Gamma \rightarrow U)$	0.38	0.41
			$m_e(\Gamma \rightarrow T)$	0.44	0.50
			$m_e(\Gamma \rightarrow Y)$	0.42	0.49

The $CaCO_3$ aragonite polymorph has also an orthorhombic unit cell. Recently performed LDA and GGA calculations [11] previewed very close indirect [$E_{G,LDA}(X \rightarrow \Gamma) = 4.00$ eV and $E_{G,GGA}(X \rightarrow \Gamma) = 4.29$ eV] and direct [$E_{G,LDA}(\Gamma \rightarrow \Gamma) = 4.01$ eV and $E_{G,GGA}(\Gamma \rightarrow \Gamma) = 4.27$ eV] energy gaps. Consequently, the substitution of carbon by germanium, which modifies the contribution to the valence electronic configuration from C-$2s^2 2p^4$ to Ge-$4s^2 4p^2$, changes the localization of the valence band maximum of the indirect transition from the point of symmetry X to S, and decreases by almost 2.0 eV the Kohn–Sham band gap energies.

In Table 3 we summarize the effective masses obtained for $CaGeO_3$. It can be seen that LDA masses are always smaller than GGA masses for electrons and holes. Hole effective masses are large (in particular, valence bands along lines to the R, U, T and Y points are too flat to allow a meaningful estimate) and very anisotropic, varying between 1 and $4.3m_0$ at the S point (m_0 is the free space electron mass). Along the $S \rightarrow \Gamma$ direction we have two degenerate bands with distinct curvatures and, therefore, two hole masses: a light hole (lh) close to $1m_0$, and a heavy hole (hh) almost 4 times larger. Electron masses, on the other hand, are smaller and almost isotropic, varying between 0.35 and $0.44m_0$ for the LDA calculation, and between 0.39 and $0.50m_0$ for the GGA calculation. A similar behavior for the hole and electron effective masses (large and anisotropic hole masses, light and almost isotropic electron masses) was observed for $CaSiO_3$ wollastonite [8].

3.3. Optical properties

Migas et al. [31] reported first-principles results for the ground-state properties, band structures, density of states and dielectric functions of Ca_2X compounds, where $X =$ Si, Ge, Sn, and Pb, considering cubic and orthorhombic phases. Their calculations were carried out using ultrasoft pseudopotentials and the full potential linearized augmented plane wave (FPLAPW) method in both LDA and GGA frameworks. Their ultrasoft pseudopotential approach is essentially the same we are employing here for structural and electronic calculations, without taking into account quasiparticle corrections. More recently, Lebègue et al. [32] recently computed the quasiparticle

properties of Ca_2Si using the all electron GW approximation based on the projector-augmented-wave method (PAQ), exploring both the orthorhombic and the cubic phases. Comparing the resulting band structures with those obtained employing the LDA, there is, as expected, a very pronounced difference of energies between the conduction and valence states using the GW approximation, as compared with the DFT results. In particular, the minimum band gap for interband transitions at the Γ point is 1.02 eV within the GW approximation, but only 0.30 eV using only DFT.

The dielectric function is affected by the quasiparticle self-energy correction and the local-field effects, due to the explicit dependence of the dielectric function $\varepsilon(\mathbf{r}, \mathbf{r}', \omega)$ on $\mathbf{r}$ and $\mathbf{r}'$ and not only on $|\mathbf{r} - \mathbf{r}'|$ [32]. For the static dielectric function quasiparticle correction is unnecessary, because it is a ground state feature. On the other hand, the dielectric constant calculated by taking into account quasiparticle corrections is useful only if excitonic effects are considered. This occurs because excitonic effects tend to shift oscillator strength toward lower energies, cancelling in part or completely the quasiparticle correction to the static dielectric function. Electron–hole interaction effects on the dielectric constant, however, are beyond the reach of computational methods due to convergence problems [33]. Beyond that, dielectric properties calculated for some calcium compounds are impaired when the pseudopotential for Ca does not take into account additional semicore electrons [34]. In view of these considerations, the results presented here for orthorhombic $CaGeO_3$ must be considered with some caution. Due to the limited computational power available to our research team, we have not considered the quasiparticle corrections and Ca semicore electrons, so the dielectric function peaks we present here must be energy shifted by an unknown amount in order to be compared with experimental results, and their intensities must be regarded only as broad indications. Keeping these facts in mind we note, however, that the peaks for the dielectric functions calculated by Lebègue et al. [32] are in general resized, but not very energy shifted, when local-field effects are included in the dielectric function calculations. Indeed, their calculated dielectric functions consider only the self-energy correction at the Γ point, adopting this value to rigidly shift the energies of all unoccupied DFT bands in order to produce an average GW correction to the band structure, arguing at the same time that the choice of the correct quasiparticle energies, instead of the DFT shifted energies, will lead only to minor corrections in the dielectric function, hardly noticeable when one looks at the calculated optical spectra. So we presume that the results we show here, despite the absence of many particle refinements and local-field effects, are useful for further experimental investigations of $CaGeO_3$ optical properties. We would like also to point out that a work similar to ours was carried out for perovskite $CaTiO_3$, and the calculated dielectric functions were found to be in good agreement with the experimental data [35].

Fig. 4 depicts the calculated real and imaginary parts of the dielectric function and optical absorption for $CaGeO_3$ with incident light polarized along different crystal directions (1 0 0 and 1 1 1) and polarized light incident on a polycrystalline sample. In both LDA and GGA approaches, the complex dielectric function of orthorhombic $CaGeO_3$ is very similar for light polarized along the crystalline directions 100, 010, and 001, but for the 111 direction the optical response was more intense as a consequence of the alignment of Ca–O dipoles with the 111 polarized electric field. The GGA calculation of the real $\varepsilon_1(\omega)$ and imaginary $\varepsilon_2(\omega)$ parts of the complex dielectric function are presented at the top and bottom of Fig. 4, respectively. The calculated static dielectric constant for polycrystalline $CaGeO_3$ is $\varepsilon_0 = 5.1$. The imaginary part $\varepsilon_2(\omega)$, depicted at the bottom part of Fig. 4, is closely related to the optical absorption, which is shown as an inset at the bottom of Fig. 4. We see some small peaks closer to the main Kohn–Sham band gap occurring at 2.3, 2.7–2.9, 3.2–3.4, and 3.7–3.9 eV, respectively. For energies between 2.3 and 7 eV, approximately, optical absorption increases slowly. Starting from 7 eV to larger energies, however, we note that the optical absorption increases more quickly.

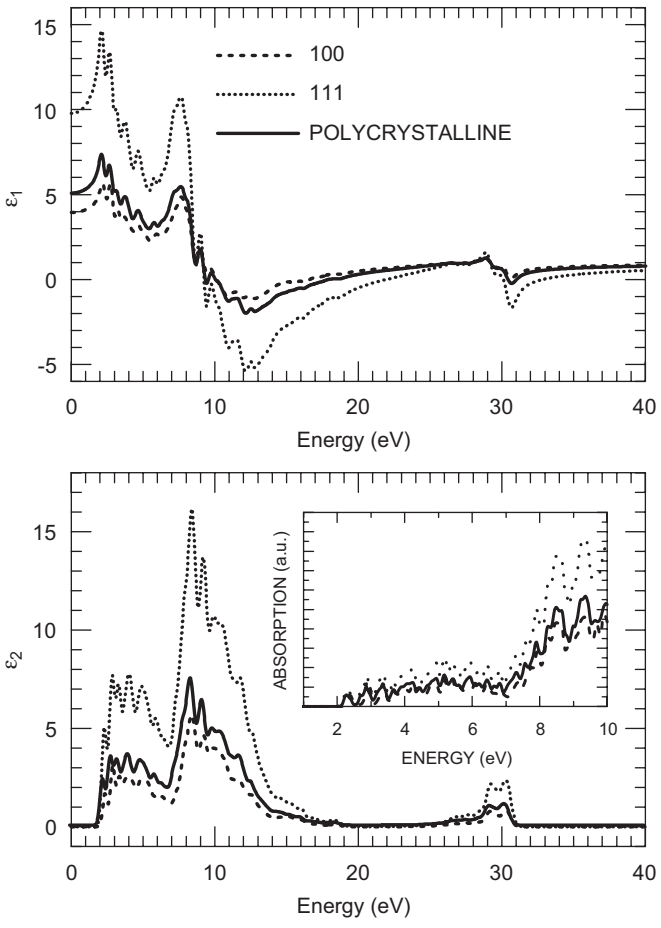

Fig. 4. Real (top) and imaginary (bottom) components of the orthorhombic $CaGeO_3$ dielectric function for polarized incident light and light incident on a polycrystalline sample. The inset depicts optical absorption $\alpha(\omega)$.

We suppose that this change of regime is due to the appearance of transitions involving mainly O-2*p* valence states and mainly Ca-4*s* conduction states for energies larger than 7 eV. The slow increase observed for energies smaller than 7 eV involves transitions between O-2*p* valence states and mainly Ge-4*s* conduction states (see Fig. 3).

4. Conclusions

In this work, we have obtained the structural, electronic and optical properties of orthorhombic $CaGeO_3$ using quantum chemical first-principles calculations. The structural parameters of orthorhombic $CaGeO_3$, calculated after geometry optimization, show a good agreement with the experimental data. The GGA approximation overestimates the actual orthorhombic $CaGeO_3$ lattice parameters by 2% at most, while the LDA lattice parameters are underestimated by practically the same amount. The smallest energy gap between valence and band conductions is indirect between the S and Γ points, corresponding for the LDA and GGA calculation to 2.31 and 1.68 eV, respectively. The $\Gamma \rightarrow \Gamma$ direct transition is 2.41 eV (LDA) and 1.75 eV (GGA). In comparison, according to the LDA calculations [8], $CaSiO_3$ presents a wide indirect band gap of 5.43 eV between the Q and Γ points, and a direct band gap of 5.52 eV for $\Gamma \rightarrow \Gamma$ transitions, while $CaCO_3$ orthorhombic (aragonite) exhibit very close indirect $X \rightarrow \Gamma$ and direct band gaps [11]. LDA effective masses are always smaller than GGA masses for electrons and holes, with hole effective masses larger and very anisotropic. Electron masses are smaller and almost isotropic. In both LDA and GGA approaches, the dielectric function of orthorhombic $CaGeO_3$ is very similar for incident light polarized along the crystalline directions 100, 010, and 001, but for the 111 direction the optical response was more intense as a consequence of the partial alignment of Ca–O electric dipoles with the 111 polarized electric field. In the energy range between 2.3 and 7 eV, approximately, optical absorption increases slowly, but from 7 eV to larger energies, optical absorption increases more quickly due to the appearance of transitions involving mainly O-2*p* valence states and mainly Ca-2*s* conduction states (for energies larger than 7 eV).

Acknowledgments

VNF, JAPC, and ELA are senior researchers from the Brazilian National Research Council CNPq, and would like to acknowledge the financial support received during the development of this work from the Grants CNPq-CTENERG 504801/2004-0 and CNPq-Rede NanoBioestruturas 555183/2005-0. J.M.H. was sponsored by a graduate fellowship from the Brazilian National Research Council (CNPq) at the Physics Department of the Universidade Federal do Rio Grande do Norte. We also thank the referees for the valuable suggestions and corrections proposed to improve this paper.

References

[1] T. Nagai, T. Yamanaka, Phys. Chem. Miner. 25 (1997) 1.
[2] B. Magyari-Köpe, L. Vitos, B. Johansson, J. Kollár, Phys. Rev. B 66 (2002) 092103.
[3] D.Y. Jung, A.R. Oganov, Phys. Chem. Miner. 32 (2005) 146.
[4] B.B. Karki, J. Crain, Geophys. Res. Lett. 25 (1998) 2741.
[5] R. Caracas, R. Wentzcovitch, G.D. Price, J. Brodho, Geophys. Res. Lett. 32 (2005) L06306.
[6] B.B. Karki, R.M. Wentzcovitch, S. de Gironcoli, S. Baroni, Phys. Rev. B 62 (2000) 14750.
[7] R.M. Wentzcovitch, N.L. Ross, G.D. Price, Phys. Earth Planet. Inter. 90 (1995) 101.
[8] J.M. Henriques, E.W.S. Caetano, V.N. Freire, J.A.P. da Costa, E.L. Albuquerque, Chem. Phys. Lett. 427 (2006) 113.
[9] A.J. Skinner, J.P. FaFemina, H.J.F. Jansen, Am. Mineral. 79 (1994) 205.
[10] D.R. Baer, D.L. Blanchard, Appl. Surf. Sci. 72 (1993) 295.
[11] S.K. Medeiros, E.L. Albuquerque, F.F. Maia Jr., E.W.S. Caetano, V.N. Freire, Chem. Phys. Lett. 430 (2006) 293.
[12] M.D. Segall, P.L.D. Lindan, M.J. Probert, C.J. Pickard, P.J. Hasnip, S.J. Clark, M.C. Payne, J. Phys. Condens. Matter. 14 (2002) 2717.
[13] P. Hohenberg, W. Kohn, Phys. Rev. 136 (1964) B864.
[14] W. Kohn, L.J. Sham, Phys. Rev. 140 (1965) A1133.
[15] R.O. Jones, O. Gunnarsson, Rev. Mod. Phys. 61 (1989) 689.
[16] O.V. Gritsenko, P.R. Schipper, E.J. Baerends, J. Chem. Phys. 107 (1997) 5007.
[17] A. Dal Corso, A. Pasquarello, A. Baldereschi, R. Car, Phys. Rev. B 53 (1996) 1180.
[18] M. Fuchs, M. Bockstedte, E. Pehlke, M. Scheffler, Phys. Rev. B 57 (1998) 2134.
[19] D. Vanderbilt, Phys. Rev. B 41 (1990) 7892.
[20] J.P. Perdew, A. Zunger, Phys. Rev. B 23 (1981) 5048.
[21] D.M. Ceperley, B.J. Alder, Phys. Rev. Lett. 45 (1980) 566.
[22] J.P. Perdew, K. Burke, M. Ernzerhof, Phys. Rev. Lett. 77 (1996) 3865.
[23] J.P. Perdew, J.A. Chevary, S.H. Vosko, K.A. Jackson, M.R. Pederson, D.J. Singh, C. Fiolhais, Phys. Rev. B 46 (1992) 6671.
[24] H.J. Monkhorst, J.D. Pack, Phys. Rev. B 13 (1976) 5188.
[25] S. Sasaki, T. Prewitt, R.C. Liebermann, Am. Mineral. 68 (1983) 1189.
[26] B.G. Pfrommer, M. Cote, S.G. Louie, M.L. Cohen, J. Comput. Phys. 131 (1997) 233.
[27] J.S. Lin, A. Qteish, M.C. Payne, V. Heine, Phys. Rev. B 47 (1993) 4174.
[28] H.A. Kramers, Nature 117 (1926) 775.
[29] R. de L. Kronig, J. Opt. Soc. Am. 12 (1926) 547.
[30] Y. Wang, D.J. Weidner, F. Guyot, J. Geophys. Res. 101 (1996) 661.
[31] D.B. Migas, L. Miglio, V.L. Shaposhnikov, V.E. Borisenko, Phys. Rev. B 67 (2003) 205203.
[32] S. Lebègue, B. Arnaud, M. Alouani, Phys. Rev. B 72 (2005) 085103.
[33] B. Arnaud, M. Alouani, Phys. Rev. B 63 (2001) 085208.
[34] M. Verstraete, X. Gonze, Phys. Rev. B 68 (2003) 195123.
[35] S. Saha, T.P. Sinha, A. Mookerjee, Eur. Phys. J. B 18 (2000) 207.